FORMULATION OF IMAGE QUALITY PREDICTION CRITERIA FOR THE VIKING LANDER CAMERA

by Friedrich O. Huck, Daniel J. Jobson,
Edward J. Taylor, and Stephen D. Wall

Langley Research Center
Hampton, Va. 23665

1. Report No. NASA TM X-2802	2. Government Accession No.	3. Recipient's Catalog No.
4. Title and Subtitle FORMULATION OF IMAGE QUALITY PREDICTION CRITERIA FOR THE VIKING LANDER CAMERA		5. Report Date September 1973
		6. Performing Organization Code
7. Author(s) Friedrich O. Huck, Daniel J. Jobson, Edward J. Taylor, and Stephen D. Wall		8. Performing Organization Report No. L-8928
9. Performing Organization Name and Address NASA Langley Research Center Hampton, Va. 23665		10. Work Unit No. 815-20-04-03
		11. Contract or Grant No.
12. Sponsoring Agency Name and Address National Aeronautics and Space Administration Washington, D.C. 20546		13. Type of Report and Period Covered Technical Memorandum
		14. Sponsoring Agency Code
15. Supplementary Notes		

16. Abstract

    Image quality criteria are defined and mathematically formulated for the prediction computer program which is to be developed for the Viking lander imaging experiment. The general objective of broad-band (black and white) imagery to resolve small spatial details and slopes is formulated as the detectability of a right-circular cone with surface properties of the surrounding terrain. The general objective of narrow-band (color and near-infrared) imagery to observe spectral characteristics is formulated as the minimum detectable albedo variation. The general goal to encompass, but not exceed, the range of the scene radiance distribution within a single, commandable, camera dynamic range setting is also considered.

17. Key Words (Suggested by Author(s)) Image quality Viking lander camera	18. Distribution Statement Unclassified — Unlimited		
19. Security Classif. (of this report) Unclassified	20. Security Classif. (of this page) Unclassified	21. No. of Pages 27	22. Price* Domestic, $3.00 Foreign, $5.50

FORMULATION OF IMAGE QUALITY PREDICTION CRITERIA

FOR THE VIKING LANDER CAMERA

By Friedrich O. Huck, Daniel J. Jobson, Edward J. Taylor,
and Stephen D. Wall
Langley Research Center

SUMMARY

Image quality criteria are defined and mathematically formulated for the prediction computer program which is to be developed for the Viking lander imaging experiment. The general objective of broad-band (black and white) imagery to resolve small spatial details and slopes is formulated as the detectability of a right-circular cone with surface properties of the surrounding terrain. The general objective of narrow-band (color and near-infrared) imagery to observe spectral characteristics is formulated as the minimum detectable albedo variation. The general goal to encompass, but not exceed, the range of the scene radiance distribution within a single, commandable, camera dynamic range setting is also considered.

INTRODUCTION

One of the primary experiments of the two Viking lander missions to Mars in 1975 is imagery, two facsimile cameras being used on each lander. The primary purpose of the imaging experiment is to spatially and (to a lesser extent) spectrally characterize the terrain which surrounds the landers. Optimization of this experiment depends not only on the camera design but also on the imaging strategy. It is, for example, generally known from the Lunar Orbiter and Surveyor missions to the Moon and the Mariner missions to Mars that image contrast of surface detail is critically dependent on illumination and viewing geometry.

Preflight predictions of image quality have been made by Rindfleisch and Willingham (refs. 1 and 2) for the Ranger missions, and by Keene (ref. 3) and Huck (ref. 4) for the Lunar Orbiter missions. These investigations have shown that a careful formulation and evaluation of the interaction between camera characteristics, mission constraints, and known or estimated surface properties can contribute significantly to a successful imaging strategy. Although these investigations and the experiences gained from the Surveyor imaging experiments are helpful in establishing an imaging strategy for the

Viking lander experiment, an image prediction analysis is nevertheless needed. This need arises because the performance characteristics of the facsimile cameras differ from previously used television and film cameras, and because mission constraints differ from previous space imaging experiments.

Of primary concern to both the Viking lander camera design and imaging strategy — as should prove typical for exploratory planetary imaging experiments in general — is the unknown nature of surface properties at the scale of observation and the limited data transmission capacity due to the long distances and spacecraft weight and power constraints. The camera must, therefore, have a good sensitivity over a wide dynamic range whereas the number of encoding levels of surface radiance must be kept low. To accommodate these two conflicting requirements, the Viking facsimile camera uses 6-bit encoding with 192 partial dynamic ranges which can be selected by 6 gains and 32 offsets. These partial dynamic ranges have a linear transfer function to provide images with good radiometric accuracy, rather than a logarithmic transfer function which would insure superficially pleasing image quality.

In addition, the Viking lander cameras feature four imaging modes (survey, high resolution, color, and near infrared) and two scan rates (matched to the data transmission rates of 16 000 bits per second to the Orbiter and 250 bits per second directly to Earth); these features result in various performance characteristics and require different viewing geometries. The cameras also have a single-line scan mode which permits an increase in radiometric sensitivity by repeatedly scanning a single line in the scene.

Preflight predictions of image quality should be conducted both experimentally and analytically. The primary advantage of experimental predictions is that results that appear in the form of images will principally be used for interpreting the results of the actual investigation, whereas the primary advantage of analytical predictions is that a wide range of conditions can readily be simulated on the computer. Thus, a handbook of images obtained under various imaging conditions and with various camera settings can probably serve the experimenter best if anticipated situations (for example, of Mars optical surface properties and camera performance characteristics) are encountered, and a flexible software program can probably serve him best if unanticipated situations are encountered that require a rapid response. The pursuit of both approaches not only combines these advantages but also provides a means for checking the results of one approach with the other.

The purpose of this paper is to provide the necessary analytical basis for developing the image quality prediction computer program for the Viking lander imaging experiment. Presented are definitions and mathematical formulations of pertinent image quality criteria as functions of optical surface properties, illumination and viewing geometry, and camera characteristics. It is important to recognize that an image quality

prediction computer program based on this analysis must be carefully compared with experimental preflight investigations before becoming operational.

SYMBOLS

A   area of a cone section, meters^2

b   normalized diameter of approximated circular area of a cone section (see eqs. (16))

c   normalized diameter of cone base, $2R_c/\beta L$

D   diameter, meters

f   lens focal length, meters

g   phase angle (see fig. 2), degrees

H   height, meters

I   current, amperes

i   integer

$J_n(\ )$ nth order Bessel function where $n = 0, 1, 2, \ldots$

k   spatial frequency, line pairs per meter

L   distance from camera lens in object space (see fig. 5(b)), meters

L(u,s)   lens spatial frequency response

ℓ distance from camera lens in image space (see fig. 5(b)), meters

m   number of binary digits used for encoding shades of gray, bits

N_λ spectral radiance, watts/meter^2-micrometer-steradian

$\hat{N}$ unit vector normal to surface

n	number of overlapping line scans
$P(v_a s)$	spatial frequency response of circular photosensor aperture
P_λ	spectral radiant power, watts/micrometer
$P_\lambda(bv_a s)$	spatial frequency distribution of circular area of a cone section
R	radius, meters
R_λ	photosensor responsivity, amperes/watt
S_λ	solar irradiance above Martian atmosphere, watts/meter^2-micrometer
S/N	ratio of average signal to root-mean-square noise
s	dimensionless variable for spatial frequency k (see eq. (15))
u	dimensionless variable for defocus (see eq. (20))
v	dimensionless variable for radius (see eq. (15))
α	target slope, degrees or radians
β	instantaneous field of view or angular resolution (see fig. 5(b)), degrees or radians
$\gamma = \cos^{-1}\left(\dfrac{s}{2}\right)$	
δ	azimuth cone angle increment (see fig. 3), degrees or radians
ϵ	angle between emitted radiation and normal to surface (see fig. 2), degrees or radians
ζ	azimuth angle between object slope and incident radiation (see fig. 2), degrees or radians
θ	azimuth angle between incident and emitted radiation (see fig. 2), degrees or radians

4

ι angle between incident radiation and normal to surface (see fig. 2), degrees or radians

λ wavelength, meters

$\xi = \dfrac{1}{2}\left(\zeta_{sh} + \psi_{sh} - \theta\right)$

$\Pi(x)$ top hat function $\left(=1 \quad \text{if} \quad |x| \leq \dfrac{1}{2}; \; =0 \quad \text{elsewhere}\right)$

ρ_λ spectral reflectivity of surface (normal albedo)

σ population deviation

$\tau_\lambda\left(\iota_0\right)$ spectral transmissivity of atmosphere

$\tau_{\lambda,s}$ spectral transmissivity of optics

ϕ illumination scattering function

ψ azimuth angle between object slope and emitted radiation (see fig. 2), degrees or radians

Ω angle defining numerical aperture (see fig. 5(b)), degrees

ω angle, radians

Subscripts:

a   photosensor aperture

c   cone

e   electronic

i   integer

ℓ lens

n	noise
o	flat surface
q	quantization
s	signal
sh	shadow
v	visible
+	brighter than flat surface
-	darker than flat surface

The symbol Δ in front of a parameter indicates a differential of that parameter. The bracket $\langle\ \rangle$ around a parameter indicates a criterion which is to be estimated. Bar over a symbol denotes an average value. A circumflex ($\char94$) over a symbol denotes a unit vector.

DEFINITION OF IMAGE QUALITY CRITERIA

The Viking lander camera (see ref. 5 and the appendix for details) has four imaging modes: survey, high resolution, color, and near infrared (IR). In the broad-band survey and high-resolution imaging modes, it is generally desirable to record small spatial details and slope variations. In the narrow-band color and IR imaging modes, it is generally desirable to record spectral variations. In addition, it is generally also desirable in all four imaging modes to encompass, but not exceed, the complete range of radiance variations in the scene with a single dynamic gain setting. The purpose of this section is to define image quality criteria which will permit the mathematical formulation of these three objectives:

(1) Knowledge of the statistical distribution (histogram) of surface radiance would allow the selection of an optimum camera dynamic range setting (that is, gain and offset as illustrated in the appendix) for the complete or a particular part of the radiance range. But the actual radiance distribution will, of course, not be known until after video data have been received from the lander. Until such data have been received, it is proposed that a minimum, mean, and maximum value of the radiance distribution be estimated, the

albedo and illumination scattering function of the scene being assumed to be uniform over the landing site. Clearly, the minimum surface radiance occurs in shadows. Since atmospheric scattering on Mars is small within the spectral range of the camera silicon photosensors (excepting, of course, a dust storm), shadows will exhibit very little radiance – certainly much less than the smallest commandable camera offset. (See appendix.) Hence, for the purpose of selecting a camera offset, minimum radiance may be defined as zero. The mean radiance is defined as the radiance of a level surface for a given viewing geometry. The maximum radiance is defined as the radiance of a surface area with a slope and slope orientation which produces highest surface reflectance, again for a given viewing geometry. Hence, mean and maximum radiance estimates are functions of surface albedo and illumination scattering function.

(2) The capability to resolve spectral variations is defined as the minimum detectable albedo variation. This minimum detectable variation is taken to be that difference in albedo which results in a ratio of signal to root-mean-square noise of 3, a level surface being assumed.

(3) The capability to resolve small spatial details and slopes is defined here as the minimum detectable cone diameter and cone slope with respect to a level surface. This criterion is based in part on a figure of merit for image quality which was first proposed in reference 1.

A right-circular cone with surface properties of the surrounding terrain seems intuitively representative of many features and has no preferred surface orientation azimuthally about its axis. If the cone angle is chosen to be steep, a condition yielding high surface contrast, then the detectability of this target becomes primarily a measure of the camera capability to resolve small detail. If the cone angle is chosen to be shallow, a condition yielding low surface contrast, then the detectability of the same target becomes primarily a measure of the camera capability to resolve small slopes.

The cone is probably also the simplest shape for this application. But it would, nevertheless, be unnecessarily complex to translate rigorously cone-surface-radiance variations into image grey-scale variations in order to estimate the detectability of a cone. Instead, the average radiance is calculated separately over those regions of the cone which are brighter than a level surface background, and those regions, including a shadow (if present), which are darker than the background. The two average reflectance values and their corresponding areas are then used as approximate target characteristics in order to formulate an expression for the ratio of signal to noise for the image of a cone.

MATHEMATICAL FORMULATION OF IMAGE QUALITY CRITERIA

Figure 1 outlines the analytical approach taken to formulate the image quality criteria which have just been discussed. Each block of this flow diagram represents a section of the analysis.

The first section specifies the angular relationships necessary to account for the dependence of surface reflectance on surface slopes and illumination and viewing geometry. The next section presents the geometry of an upright cone, which was selected to represent small spatial detail and slope variations. Reflectance variations of the cone are approximated in the third section by an average reflectance value for those sections of the cone which have a higher reflectance than a level background surface and another average reflectance value for those sections which have a lower reflectance (including shadow, if present). The fourth section formulates the resultant spectral surface radiance and the radiant power incident on the camera, and the fifth section formulates the camera response to this input signal. The sixth section describes the noise generated by the photosensor and preamplifier, and the quantization error caused by encoding the electrical signal for digital transmission. The last section formulates the desired image quality parameters.

Viewing Geometry

Figure 2 defines the angular relationships between surface slopes and illumination and viewing geometry. The illumination scattering function $\phi_\lambda(\epsilon, \iota, g)$, which accounts for the dependence of surface reflectance on this geometry, is a function of the angle ι between incident radiation and surface normal, the angle ϵ between emitted radiation and surface normal, and the phase angle g between incident and emitted radiation. These three angles can be determined from the following relationships:

$$\cos g = \cos \epsilon_0 \cos \iota_0 + \sin \epsilon_0 \sin \iota_0 \cos \theta \tag{1}$$

$$\cos \iota = \cos \alpha \cos \iota_0 - \sin \alpha \sin \iota_0 \cos \zeta \tag{2}$$

$$\cos \epsilon = \cos \alpha \cos \epsilon_0 - \sin \alpha \sin \epsilon_0 \cos \psi \tag{3}$$

where ϵ_0 and ι_0 are the emission and incident angles, respectively, for a level surface $\left(\text{with normal } \hat{N}_0\right)$, α is the angle of a surface element with respect to a level surface $\left(\text{and with normal } \hat{N}\right)$, θ is the azimuth angle between incident radiation and camera optical axis, and ζ and ψ are azimuth angles of the plane formed by the

normals $\hat{N}$ and $\hat{N}_0$ with respect to incident radiation and camera, respectively. The three azimuth angles are related by

$$\theta + \zeta + \psi = 2\pi \tag{4}$$

Target Geometry

Geometric relationships required to describe the reflectance variations of a right circular cone have been derived in reference 1 and are generalized here to include viewing geometries for that part of the cone, including its shadow (if present), which is obscured from the camera view by the cone itself. Only an upright cone is considered here, whereas reference 1 also considers an inverted cone.

Figure 3 illustrates the geometry of an upright cone with a base of radius R_c, a height H, and a slope α so that

$$\alpha = \tan^{-1} \frac{H}{R_c} \qquad\qquad \left(0 < \alpha < \frac{\pi}{2}\right) \tag{5}$$

An area element about a generator of the cone and with normal $\hat{N}$ is given in terms of the azimuth angle increment δ as

$$\Delta A = \frac{\delta R_c^2}{2 \cos \alpha} \tag{6}$$

If $\iota_0 \geqq 90^\circ - \alpha$, a shadow is cast by the cone on a level surface (as shown shaded in fig. 3(a)) for $-\zeta_{sh} < \zeta < \zeta_{sh}$, where $\zeta_{sh} = \cos^{-1}(1/\tan \alpha \tan \iota_0)$; this shadow has an area

$$A_{sh} = R_c^2 \left(\tan \zeta_{sh} - \zeta_{sh}\right) \tag{7a}$$

Similarly, if $\epsilon_0 \geqq 90^\circ - \alpha$, a "visual" shadow is formed (fig. 3(b)) which obscures part of the cone and cone shadow (if there is one) from the camera. It is assumed that the rays of light intercepted by the camera are parallel instead of convergent since only small targets are of interest and the convergence angle is therefore small. Under this condition, area elements ΔA of the cone not visible to the camera are defined by the range $-\psi_{sh} < \psi < \psi_{sh}$, where $\psi_{sh} = \cos^{-1}(1/\tan \alpha \tan \epsilon_0)$. The shadow area still visible to the camera becomes (see fig. 4)

$$A_{v,sh} = R_c^2\left(\tan \zeta_{sh} - \zeta_{sh} - \tan \xi + \xi\right) \tag{7b}$$

where $\xi = \frac{1}{2}\left(\zeta_{sh} + \psi_{sh} - \theta\right)$.

Several geometries must be accounted for when equation (7b) is used. The azimuth angle θ between incident radiation and camera optical axis must always be chosen so that $\theta < \pi$. When $\theta \gtrsim \zeta_{sh} + \psi_{sh}$, the "visual" shadow does not overlap any part of the illumination shadow, and equation (7b) reduces to equation (7a). When $\theta + \zeta_{sh} \lesssim \psi_{sh}$, the illumination shadow is completely contained within the visual shadow, and the angle ξ must be set equal to ζ_{sh} so that $A_{sh} = 0$. When $\theta + \psi_{sh} \lesssim \zeta_{sh}$, the visual shadow is completely contained within the illumination shadow, and the angle ξ must be set equal to ψ_{sh}.

Approximate Target Characteristics

Target and background are considered to be of the same material so that the variation in cone reflectance with azimuth angle is dependent only on the illumination scattering function. But it would still be exceedingly difficult to translate this reflectance variation exactly into an image signal. The reflectance variation is therefore approximated by an average reflectance of that part of the cone which has a higher than background reflectance and another part which has a lower than background (including shadow) reflectance.

The total projected area of all cone sections which have a higher than background reflectance and are visible to the camera may be expressed as

$$A_+ = \Delta A \sum_i \cos \epsilon_i = \frac{R_c^2 \delta}{2 \cos \alpha} \sum_i \cos \epsilon_i \qquad \left(\phi_i(\epsilon, \iota, g) > \phi_o\right) \tag{8}$$

where $\phi_o \equiv \phi\left(\epsilon_o, \iota_o, g\right)$. The average value of the illumination scattering function of this area becomes

$$\phi_+ = \frac{\Delta A}{A_+} \sum_i \phi_i(\epsilon, \iota, g)\cos \epsilon_i = \frac{\displaystyle\sum_i \phi_i(\epsilon, \iota, g)\cos \epsilon_i}{\displaystyle\sum_i \cos \epsilon_i} \qquad \left(\phi_i(\epsilon, \iota, g) > \phi_o\right) \tag{9}$$

Similarly, the total projected area of all cone sections, including the shadow cast by the cone on a level surface (if present), which have a lower than background reflectance and are visible to the camera may be expressed as

10

$$A_- = \Delta A \sum_i \cos \epsilon_i + A_{sh} \cos \epsilon_o$$

$$= R_c{}^2 \left[\frac{\delta}{2 \cos \alpha} \sum_i \cos \epsilon_i + \left(\tan \zeta_{sh} - \zeta_{sh} - \tan \xi + \xi \right) \cos \epsilon_o \right]$$

$$\left(\phi_i(\epsilon, \iota, g) < \phi_o \right) \qquad (10)$$

The average value of the illumination scattering function of this area becomes

$$\phi_- = \frac{\Delta A}{A_-} \sum_i \phi_i(\epsilon, \iota, g) \cos \epsilon_i$$

$$= \frac{\delta \sum\limits_i \phi_i(\epsilon, \iota, g) \cos \epsilon_i}{\delta \sum\limits_i \cos \epsilon_i + 2 \cos \alpha \cos \epsilon_o \left(\tan \zeta_{sh} - \zeta_{sh} - \tan \xi + \xi \right)}$$

$$\left(\phi_i(\epsilon, \iota, g) < \phi_o \right) \qquad (11)$$

Reflectance from the shadow is assumed to be negligible.

Spectral Radiance and Radiant Power

The spectral radiance N_λ of a surface is generally given by (ref. 6)

$$N_\lambda = \frac{1}{\pi} S_\lambda \tau_\lambda(\iota_o) \, \rho_\lambda \phi_\lambda(\epsilon, \iota, g) \qquad (12)$$

where S_λ is the solar irradiance, $\tau_\lambda(\iota_o)$ is the transmissivity of the atmosphere, and ρ_λ is the reflectivity (normal albedo) of the surface. $\left(\text{If } \rho_\lambda \text{ is defined as bond albedo,} \right.$ then the factor $\frac{1}{\pi}$ should be replaced by $\frac{2}{3\pi}$. (See ref. 7.)$\left.\right)$

The spectral radiant power reaching the camera photosensor is (ref. 8)

$$P_\lambda = \left(\frac{\pi}{4} \right)^2 \beta^2 D_\ell{}^2 \tau_{\lambda,s} N_\lambda = \frac{\pi}{16} \beta^2 D_\ell{}^2 S_\lambda \tau_\lambda(\iota_o) \, \rho_\lambda \tau_{\lambda,s} \phi_\lambda(\epsilon, \iota, g) \qquad (13)$$

where β is the camera instantaneous field of view or angular resolution; D_ℓ, the objective lens diameter; and $\tau_{\lambda,s}$, the transmissivity of the optics and spectral filters.

To obtain the spectral radiant power $P_{\lambda,o}$ of a level surface, the function $\phi_\lambda(\epsilon, \iota, g)$ in equation (13) may be replaced by ϕ_o. To obtain the spectral-radiant-power

difference between the level surface and the brighter than background cone area $\Delta P_{\lambda,+}$ and the darker than background area $\Delta P_{\lambda,-}$, the function $\phi_\lambda(\epsilon,\iota,g)$ may be replaced in equation (13) by $\Delta\phi_+ = \phi_+ - \phi_0$ and $\Delta\phi_- = \phi_0 - \phi_-$, respectively.

Imaging Process

The next step is to formulate the method by which the facsimile camera translates the radiance variations formulated in the foregoing sections into an electrical signal. A basic configuration of the camera is shown in figure 5. Radiation from the scene is captured by the scanning mirror and objective lens and projected onto a plane which contains the photosensor aperture. The photosensor — in this case, a silicon photodiode — converts the radiation falling on the aperture into an electrical current. As the mirror rotates, the imaged scene moves past the aperture and permits the aperture to scan vertical strips. The camera rotates slowly in azimuth so that the entire scene of interest is scanned.

The line-scan imaging process of the facsimile camera has been formulated in reference 8, and all pertinent optical characteristics have been presented in reference 9. Results from these references are used here in the notation of the present report without detailed derivations, and effects of line-scan sampling, such as possible aliasing (ref. 8), are not considered.

The spectral radiant power $P_{\lambda,0}$ reaching the photosensor aperture from a surface of uniform radiance is converted by the photosensor into a current of magnitude

$$I_0 = \int_0^\infty P_{\lambda,0} R_\lambda \; d\lambda \tag{14}$$

where R_λ is the spectral responsivity of the photosensor.

In order to formulate the signal current $\Delta I_\pm$ generated by the spatially varying spectral radiant power $\Delta P_{\lambda,\pm}$ of the target cone, it is convenient to express the cone radius in terms of the camera instantaneous field of view β (see fig. 5(b)) so that $R_c = \frac{c}{2}\beta L$, where c is a constant and L is the distance from the target to the camera. It is furthermore convenient to assume the two cone areas A_+ and A_- (as given by eqs. (8) and (10), respectively) to be circular in shape with diameters D_+ and D_-, respectively, so that $A_\pm = \frac{\pi}{4}D_\pm^2$. Circular symmetry permits the use of the one-dimensional Hankel transform instead of the two-dimensional Fourier transform, and leads to a significant reduction of computational requirements. This assumption is justifiable because most of the radiant power contained in the spatial frequency distribution of the cone radiance is generally clustered around the lower spatial frequencies. The

assumption is also consistent with the earlier approximation of cone radiance variations by two average values.

The spatial frequency distribution of the target spectral radiant power (in image space) may then be given by the Hankel transform of a circular area with radius $b_{\pm}v_a$ as

$$\Delta P_\lambda\left(b_{\pm}v_a s\right) = \Delta P_{\lambda,\pm} \frac{2\pi \displaystyle\int_0^{b_{\pm}v_a} J_0(vs)v\,dv}{\displaystyle\int_0^{2\pi}\int_0^{b_{\pm}v_a} v\,dv\,d\omega} = \Delta P_{\lambda,\pm} \frac{2J_1\left(b_{\pm}v_a s\right)}{b_{\pm}v_a s} \tag{15}$$

where

$$v_a = \frac{2\pi}{\lambda} R_a \sin \Omega \approx \frac{2\pi}{\lambda}\left(\frac{D\ell}{2\ell_a}\right)R_a \approx \frac{\pi}{\lambda}\left(\frac{D\ell}{2}\right)\beta$$

$$s = \frac{\lambda}{\sin \Omega} k \approx \lambda\left(\frac{2\ell}{D\ell}\right)k$$

and

$$b_{\pm} = \frac{D_{\pm}}{\beta L} = \frac{cD_{\pm}}{2R_c} = c\sqrt{\frac{A_{\pm}}{\pi R_c^2}} \tag{16a}$$

Upon proper substitution of equations (8b) and (10b), equation (16a) becomes

$$b_{+} = c\left(\frac{\delta}{2\pi \cos \alpha} \sum_i \cos \epsilon_i\right)^{1/2} \qquad \left(\phi_i(\epsilon,\iota,g) > \phi_0\right) \tag{16b}$$

$$b_{-} = c\left[\frac{\delta}{2\pi \cos \alpha} \sum_i \cos \epsilon_i + \frac{1}{\pi}(\tan \zeta_{sh} - \zeta_{sh} - \tan \xi + \xi)\cos \epsilon_0\right]^{1/2}$$

$$\left(\phi_i(\epsilon,\iota,g) < \phi_0\right) \tag{16c}$$

The signal current generated by the photosensor now may be expressed as

$$\Delta I_{\pm}\left(u,v_a;b_{\pm},v\right) = \int_0^\infty \int_0^\infty R_\lambda\, \Delta P_\lambda\left(b_{\pm}v_a s\right) P\left(v_a s\right) L(u,s) J_0(vs)\, s\, ds\, d\lambda \tag{17}$$

where $P\left(v_a s\right)$ and $L(u,s)$ are the spatial frequency response of the photosensor aperture and lens, respectively.

The spatial frequency response of the circular photosensor aperture with radius v_a is

$$P(v_a s) = \frac{2\pi \int_0^{v_a} J_0(vs) v \, dv}{\int_0^{2\pi} \int_0^{v_a} v \, dv \, d\omega} = \frac{2J_1(v_a s)}{v_a s} \tag{18}$$

The spatial frequency response of the lens is (ref. 10)

$$\begin{aligned} L(u,s) = \frac{4}{\pi u s} \cos\left(\frac{1}{2} us^2\right) &\left\{ \gamma J_1(us) + \frac{1}{2}\sin 2\gamma\left[J_1(us) - J_3(us)\right]\right. \\ &\left. - \frac{1}{4}\sin 4\gamma\left[J_3(us) - J_5(us)\right] + \ldots \right\} \\ - \frac{4}{\pi u s}\sin\left(\frac{1}{2}us^2\right) &\left\{ \sin\gamma\left[J_0(us) - J_2(us)\right]\right. \\ &\left. - \frac{1}{3}\sin 3\gamma\left[J_2(us) - J_4(us)\right] + \frac{1}{5}\sin 5\gamma\left[J_4(us) - J_6(us)\right] - \ldots \right\} \end{aligned} \tag{19a}$$

where $\gamma = \cos^{-1}\left(\frac{s}{2}\right)$. As the photosensor aperture approaches focus ($u = 0$), the lens response becomes

$$L(0,s) = \frac{1}{\pi}(2\gamma - \sin 2\gamma) \tag{19b}$$

The dimensionless variable u is a measure of defocus and is given by (fig. 5(b))

$$u = \frac{2\pi}{\lambda} \Delta\ell \tan\Omega \sin\Omega \approx \frac{\pi}{2\lambda}\Delta\ell\left(\frac{D_\ell}{\ell}\right)^2 \tag{20}$$

where $\Delta\ell = \left|\ell_i - \ell_a\right|$.

Since most of the functions inside the Hankel transform of equation (17) are dependent on wavelength, the spatial frequency response of the camera cannot, in a rigorous formulation, be separated from its spectral response. However, such a rigorous formulation would lead to unnecessarily difficult computations for the present purpose. It is sufficient here to evaluate the Hankel transform only at a single wavelength; namely, the surface radiance and camera response weighted average wavelength $\bar{\lambda}$

$$\bar{\lambda} = \frac{\displaystyle\sum_i \lambda_i S_{\lambda,i} \tau_{\lambda,i}(\ell_0)\rho_{\lambda,i}R_{\lambda,i}\tau_{\lambda,s,i}}{\displaystyle\sum_i S_{\lambda,i}\tau_{\lambda,i}(\ell_0)\rho_{\lambda,i}R_{\lambda,i}\tau_{\lambda,s,i}} \tag{21}$$

14

Separating spectral and spatial integration in equation (17) and averaging over the circular image area of radius $b_{\pm}v_a$, this equation may be approximated by (ref. 9)

$$\Delta I_{\pm}(u,v_a;b_{\pm}) = \int_0^{\infty} \Delta P_{\lambda,\pm} R_{\lambda}\, d\lambda \left[\int_0^{b_{\pm}v_a} \int_0^{\infty} \frac{2J_1(b_{\pm}v_a s)}{b_{\pm}v_a s} \frac{2J_1(v_a s)}{v_a s} L(u,s) J_0(us)\, s\, ds\, v\, dv \right]\Bigg|_{\lambda=\bar{\lambda}}$$

$$= \int_0^{\infty} \Delta P_{\lambda,\pm} R_{\lambda}\, d\lambda \left\{ \frac{b_{\pm}^2 v_a^2}{2} \int_0^{\infty} \left[\frac{2J_1(b_{\pm}v_a s)}{b_{\pm}v_a s}\right]^2 \left[\frac{2J_1(v_a s)}{v_a s}\right] L(u,s)\, s\, ds \right\}\Bigg|_{\lambda=\bar{\lambda}} \Pi\left(\frac{v}{2b_{\pm}v_a}\right)$$

(22)

When $b_{\pm} < 1$, then the term $\dfrac{b_{\pm}^2 v_a^2}{2}$ located in front of the spatial frequency integral is to be replaced by $\dfrac{v_a^2}{2}$.

Noise

In addition to converting the radiation falling on the aperture into an electrical video signal and amplifying it, the photosensor and preamplifier also generate random electrical noise. The root-mean-square magnitude of this noise is designated herein as $I_{e,n}$. In the single-line scan mode of the camera, the effective value of this noise can be reduced to the value

$$I_{e,n}(n) = \frac{I_{e,n}}{\sqrt{n}}$$

(23)

where n is the number of line scans.

After the electrical signal has been amplified, it is sampled and quantized for digital transmission, which causes a so-called "quantization error." For m ($=6$) bit binary encoding, the root-mean-square noise value $I_{q,n}(m)$ of the quantization error is (ref. 11)

$$I_{q,n}(m) = \frac{I_{max} - I_{min}}{\sqrt{12}\, 2^m} = \frac{I_{max} - I_{min}}{222}$$

(24)

where I_{max} and I_{min} are the maximum and minimum currents encompassed by the camera dynamic range or gain setting.

Hence, the total root-mean-square value of camera noise may be expressed as

$$I_n = \left[I_{e,n}^2(n) + I_{q,n}^2(m) \right]^{1/2}$$

(25)

Image Quality Criteria

Based on the foregoing results, it is now possible to formulate the three desired image quality criteria; namely, scene radiance distribution, minimum detectable albedo difference, and minimum detectable cone diameter and slope. Since the spectral dependence of the illumination scattering function is not important here, it should generally be sufficient to evaluate $\phi_\lambda(\epsilon,\iota,g)$ only at the wavelength $\bar\lambda$ as given by equation (21).

Estimates of scene radiance distribution.- Important parameters of the scene brightness distribution which are to be estimated are the minimum, mean, and maximum radiance which can occur as a function of the illumination scattering function, a uniform albedo being assumed. Since it is always possible to find surface conditions which generate shadows, the minimum signal is defined as $\langle I_{min}\rangle \equiv 0$. The mean video signal is taken to be that of a flat surface, that is,

$$\langle I_{mean}\rangle \equiv I_0 = \int_0^\infty P_{\lambda,o}R_\lambda \, d\lambda \tag{26}$$

and the maximum video signal is estimated to be that of a surface slope oriented to yield the highest possible surface reflectance for a given viewing geometry. The estimated maximum level may, therefore, be expressed as

$$\langle I_{max}\rangle \equiv \int_0^\infty P_{\lambda,max}R_\lambda \, d\lambda \tag{27}$$

where, from equation (13),

$$P_{\lambda,max} = \frac{\pi}{16} \beta^2 D_\ell^{\,2} S_\lambda \tau_\lambda(\iota_0) \, \rho_\lambda \tau_{\lambda,s} \phi_{\lambda,max}(\epsilon,\iota,g)$$

Consequently, it is necessary to find the maximum possible value of $\phi_\lambda(\epsilon,\iota,g)$ as a function of surface slope α and orientation ζ. A brute force method would be to compute $\phi_\lambda(\epsilon,\iota,g)$ for a wide range of α and ζ, and then to select the maximum value.

Minimum detectable albedo difference.- Three assumptions are made: (1) the surface is assumed to be level so that equation (14) can be used to calculate the camera signal, (2) the surface albedo is assumed to be constant over the narrow wavelength range of the camera spectral filters so that the albedo term can be moved outside the wavelength integral, and (3) the albedo difference must be three times the root-mean-square noise value in order to be detected. Hence, solving the ratio of signal (eq. (14)) to noise (eq. (25)) equal to 3 for ρ_λ, the minimum detectable albedo difference $\langle \Delta\rho_{\bar\lambda}\rangle$ may be formulated as

$$\left\langle \Delta\rho_{\bar{\lambda}} \right\rangle \equiv \frac{48 I_n}{\pi\beta^2 D_\ell{}^2 \phi_{\bar{\lambda},o} \int_0^\infty S_\lambda \tau_\lambda(\iota_o) \, \tau_{\lambda,s} R_\lambda \, d\lambda} \tag{28}$$

<u>Minimum detectable cone diameter and slope.</u>- The signal level of the brighter than background area S_+ and darker than background area S_- may be given from equation (22) in the form

$$\Delta I_\pm = \int_0^\infty \Delta P_\lambda R_\lambda \, d\lambda \left\{ \frac{b_\pm{}^2 v_a{}^2}{2} \int_0^\infty \left[\frac{2J_1(b_\pm v_a s)}{b_\pm v_a s} \right]^2 \left[\frac{2J_1(v_a s)}{v_a s} \right] L(u,s) \, s \, ds \right\} \Bigg|_{\lambda=\bar{\lambda}} \tag{29}$$

The total average signal current excursion is $\Delta I = \Delta I_+ + \Delta I_-$.

The accuracy to which this signal can be measured depends not only on the system noise but also on the size of the image area. This is simply because the larger the image area the more picture elements (or samples of the signal) it contains. According to the central limit theorem, the mean of a sample of size n has a standard deviation $\sigma/\sqrt{n}$ if σ is the population deviation. Here σ is the total root-mean-square camera noise current I_t, and the number of independent samples n is the ratio of image area over picture-element area, that is,

$$n = \pi\left(b_+{}^2 + b_-{}^2\right) \frac{v_a{}^2}{\pi v_a{}^2} = b_+{}^2 + b_-{}^2$$

Consequently, the ratio of average signal to root-mean-square noise of a cone image may be formulated as

$$\left\langle \frac{S}{N} \right\rangle = \frac{\Delta I_+ + \Delta I_-}{I_n} \sqrt{b_+{}^2 + b_-{}^2} \tag{30}$$

In order to determine favorable lighting and viewing geometries, it should often be sufficient to evaluate equation (30) for a fixed cone slope α and normalized cone diameter $c = \dfrac{2R_c}{\beta L}$. However, if it is desirable to determine the minimum detectable cone slope, the procedure should be to specify c and then to find the slope α which yields a ratio of signal to noise S/N of 3. Or if it is desirable to determine the minimum detectable cone diameter, the procedure should be to specify α and then to find the normalized cone diameter c which yields $S/N = 3$. Both procedures require reiterative evaluations of equation (30) until a solution with desired accuracy is found.

CONCLUDING REMARKS

Image quality criteria were defined and mathematically formulated for the prediction computer program which is to be developed for the Viking lander imaging experiment. To define specific image quality criteria, it was stipulated that it is generally desirable to observe small spatial details and slopes in monospectral (black and white) images and to observe small spectral albedo variations in multispectral (color and infrared (IR)) images. In addition, it was stipulated that it is generally also desirable to encompass the entire radiance variations of the scene in all images. Because of the limited number of available encoding levels and the potentially wide range of scene radiance, trade-offs may frequently have to be made between resolving small radiance variations and encompassing the complete radiance range.

To aid in determining these trade-offs for the selection of camera gain and offset settings prior to the reception of Mars surface imagery data, three points of the statistical distribution (histogram) of surface radiance were estimated as follows: A minimum radiance was taken to be zero, since shadows will exhibit very little radiance for the small atmospheric scattering on Mars in the camera silicon photosensor wavelength range. A mean radiance was taken to be that of a level surface and a maximum radiance was taken to be that of a surface area with a slope and slope orientation which produces the highest possible value of the surface illumination scattering function.

The capability to resolve spatial details and slopes was formulated as the minimum detectable diameter and slope, respectively, of a right-circular cone. For steep angles, yielding high contrast, this target simulates small detail, and for shallow angles, yielding low contrast, this target simulates small slopes.

The capability to resolve spectral variations was formulated as the minimum detectable albedo variation, a level terrain being assumed for computing the lighting and viewing geometry dependent surface illumination scattering function.

An image quality prediction computer program based on the criteria formulated in this paper must be carefully compared with images obtained with the Viking lander camera before being certified for use as operational software. Such comparison may lead to changes and additions to these criteria which could improve the value of the operational software.

Langley Research Center,
National Aeronautics and Space Administration,
Hampton, Va., May 16, 1973.

APPENDIX

CAMERA CHARACTERISTICS

Camera characteristics are summarized here to permit preliminary evaluations of image quality parameters. Most data are taken from the VLIS Image Quality Analysis Report (ref. 12). These data are preliminary and subject to change upon evaluation of a developed camera. Some of these data may also have to be modified during the mission if camera calibration and engineering data reveal a change in performance characteristics.

Pertinent characteristics of the four camera imaging modes are given in table I. The objective lens aperture diameter is $D_\ell = 0.95$ cm and focal length is $f = 5.25$ cm. The total average transmissivity of window and optics is $\tau_\ell = 0.7$.

The electronic noise current is approximately 10^{-14} ampere$/\sqrt{\text{hertz}}$. It should be noted, however, that the noise current varies with the amount of radiant power incident on the photosensor if the incident radiation is high, and yields a significant increase in noise current in the survey mode under some imaging conditions.

Camera gains and offsets are illustrated in figure 6. The actual gains may be slightly different for each one of the photosensors and preamplifiers. These gain differences will have to be included in the final prediction program.

Figure 7 presents a nominal responsivity curve for the silicon photosensor. This responsivity may vary significantly, especially in the near infrared (IR), as a result of long-term nuclear radiation exposure from the lander radioactive thermonuclear generators, and as a function of the photosensor array temperature. These factors must be included in the final prediction program.

Figure 8 presents smoothed transmittance curves for the spectral filters. Final curves must be used when they become available.

REFERENCES

1. Rindfleisch, T.; and Willingham, D.: A Figure of Merit Measuring Picture Resolution. Tech. Rep. No. 32-666 (Contract No. NAS 7-100), Jet Propulsion Lab., California Inst. Technol., Sept. 1, 1965.

2. Rindfleisch, T.; and Willingham, D.: A Figure of Merit Measuring Picture Resolution. Advances in Electronics and Electron Physics, Vol. 22A, Academic Press, 1966, pp. 341-354.

3. Keene, George T.: Lunar Photo Study. Z-3841 (Contract NAS 9-3826), Eastman Kodak Co., Oct. 1, 1965. (Available as NASA CR-65190.)

4. Huck, Friedrich O.: A Lighting Strategy for Lunar Orbiter Mission Design. NASA TN D-4501, 1968.

5. Beal, Robert C.: Implementation of the 1975 Mars Viking Lander Cameras. Instrumentation in Astronomy, Soc. Photo-opt. Instrum. Eng., 1972, pp. 181-187.

6. Nicodemus, Fred E.: Radiance. Amer. J. Phys., vol. 31, no. 5, May 1963, pp. 368-377.

7. Hapke, Bruce W.: A Theoretical Photometric Function for the Lunar Surface. J. Geophysics Res., vol. 68, no. 15, Aug. 1, 1963, pp. 4571-4586.

8. Katzberg, Stephen J.; Huck, Friedrich O.; and Wall, Stephen D.: An Investigation of Photosensor Aperture Shaping in Facsimile Cameras. NASA TN D-6882, 1972.

9. Huck, Friedrich O.; and Lambiotte, Jules J., Jr.: A Performance Analysis of the Optical-Mechanical Scanner as an Imaging System for Planetary Landers. NASA TN D-5552, 1969.

10. Hopkins, H. H.: The Frequency Response of a Defocused Optical System. Proc. Roy. Soc. (London), ser. A, vol. 231, no. 1184, July 19, 1955, pp. 91-103.

11. Carlson, A. Bruce: Communications Systems. An Introduction to Signals and Noise in Electrical Communication. McGraw-Hill Book Co., c.1968.

12. Anon.: VLIS Image Quality Analysis Report. 2874-VLC-349 (Contract GCO-607004), Itek Corp., Oct. 1972.

TABLE I.- CAMERA CHARACTERISTICS

Characteristics	Survey	Color and infrared (IR)	High resolution
Instantaneous field of view, deg	0.12	0.12	0.04
Photosensor aperture diameter, cm	0.0114	0.0114	0.0038
Photosensor aperture distance from lens, cm	5.325	5.325	5.40, 5.35, 5.31, 5.27
In-focus distance, m	3.7	3.7	1.9, 2.7, 4.5, 13.3
Field of view per frame			
Vertical, deg	61.44	61.44	20.48
Azimuth, deg, minimum; maximum	2.5;342.5	2.5;342.5	2.5;342.5
Electronic bandwidth			
Rapid scan, Hz	1600	1600	1600
Slow scan, Hz	25	25	25
Picture elements per line scan	512	512	512
Picture elements per azimuth step	512	1536	512
Time per azimuth step			
Rapid scan, sec	0.213	0.639	0.213
Slow scan, sec	13.632	40.896	13.632
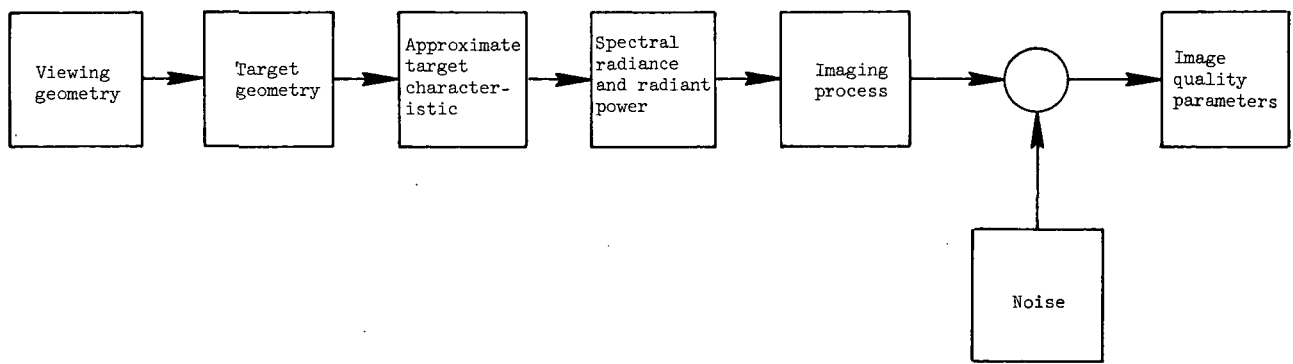
Figure 1.- Flow diagram of image quality analysis.
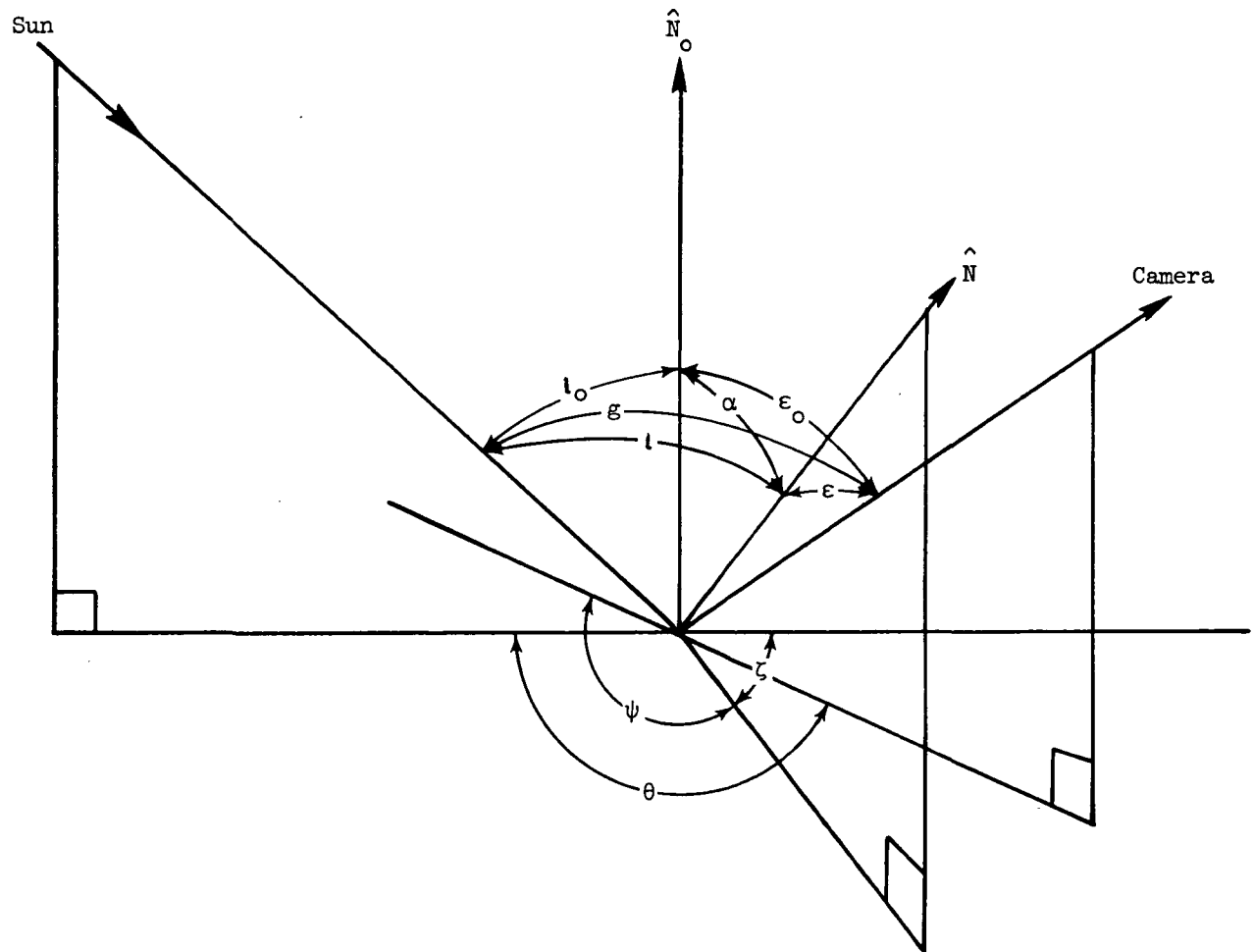
Figure 2.- Illumination and viewing geometry.
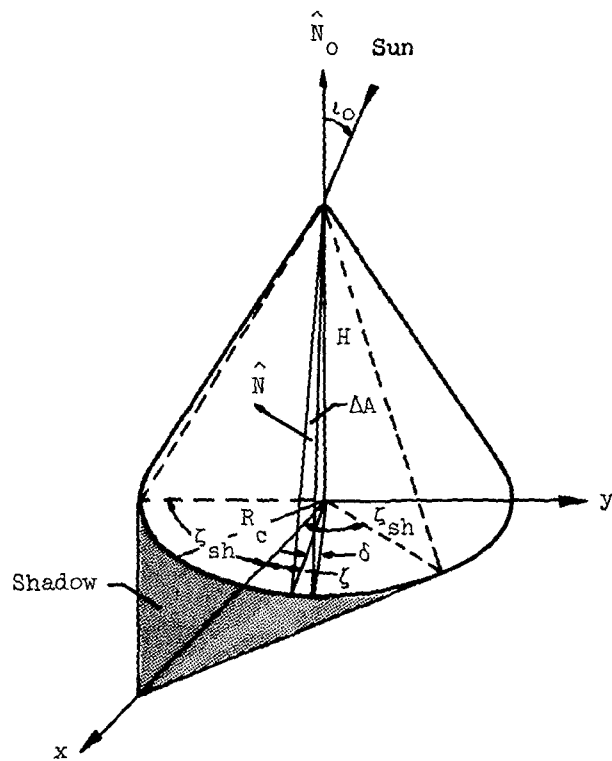
(a) Geometry for incident radiation.
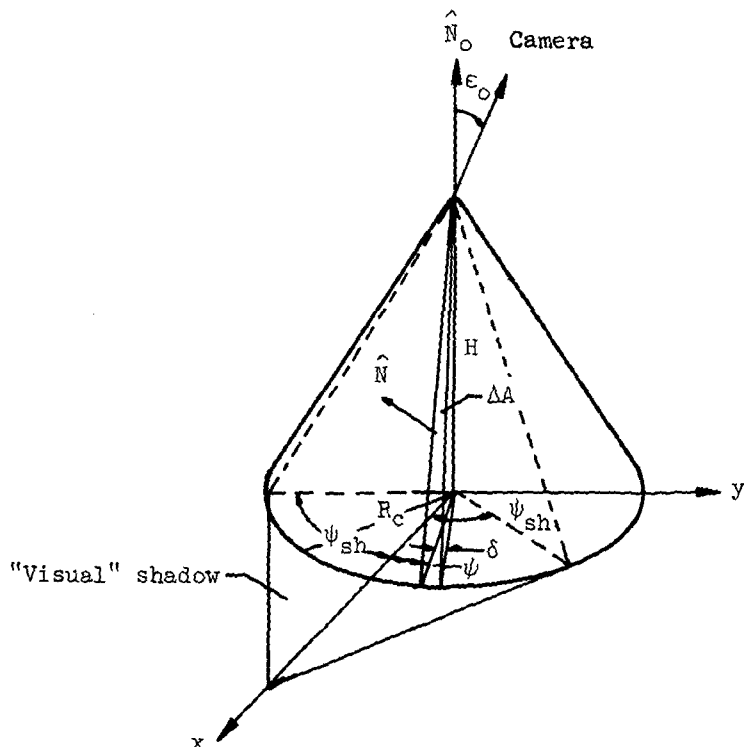
(b) Geometry for emitted radiation.

Figure 3.- Cone geometry.
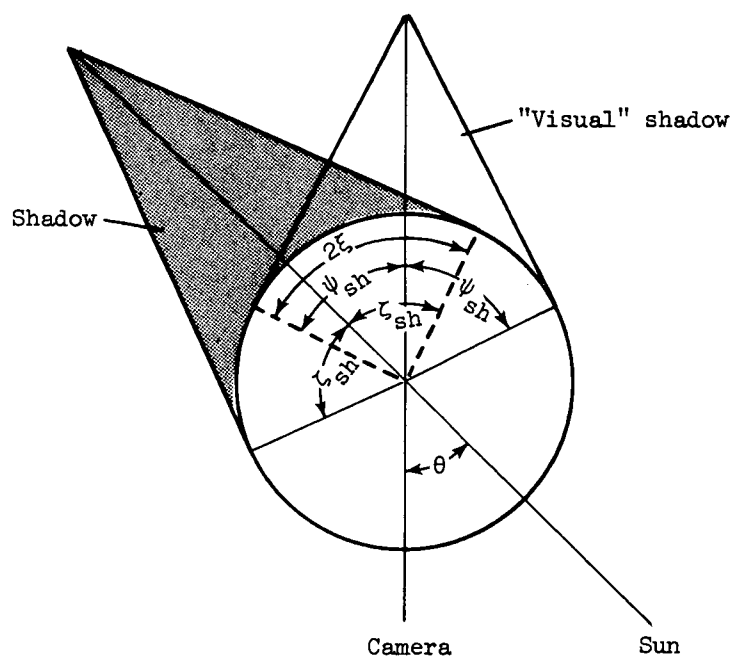
Figure 4.- Top view of cone geometry.
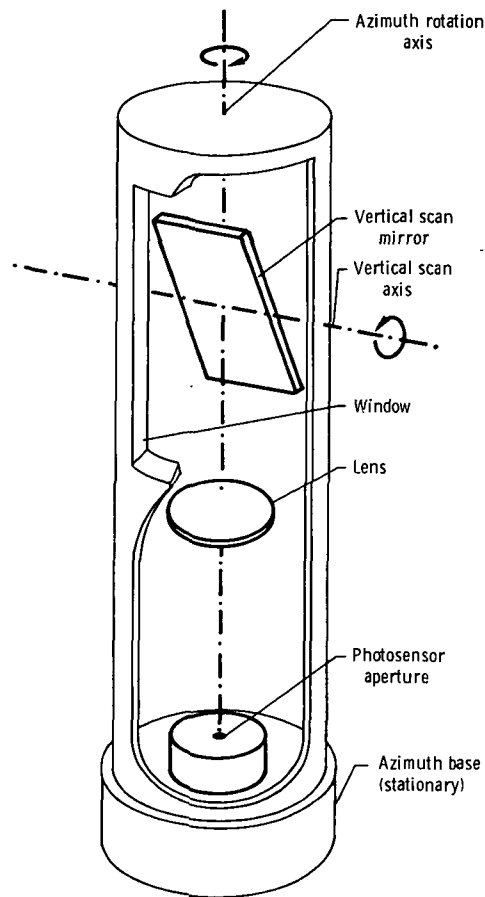
(a) Basic configuration.
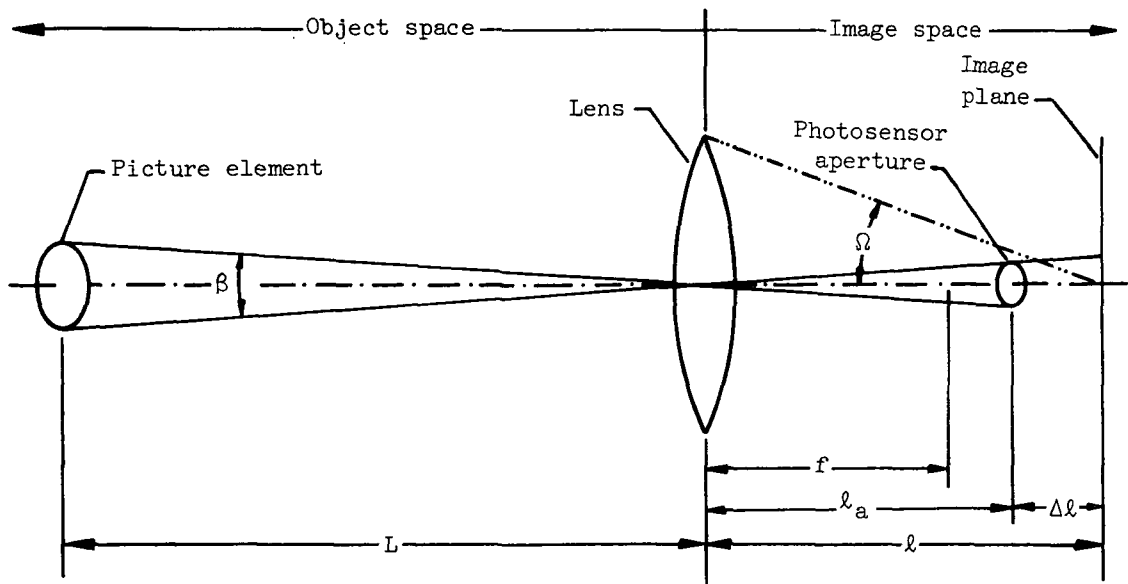


(b) Optical geometry.

Figure 5.- Facsimile camera.
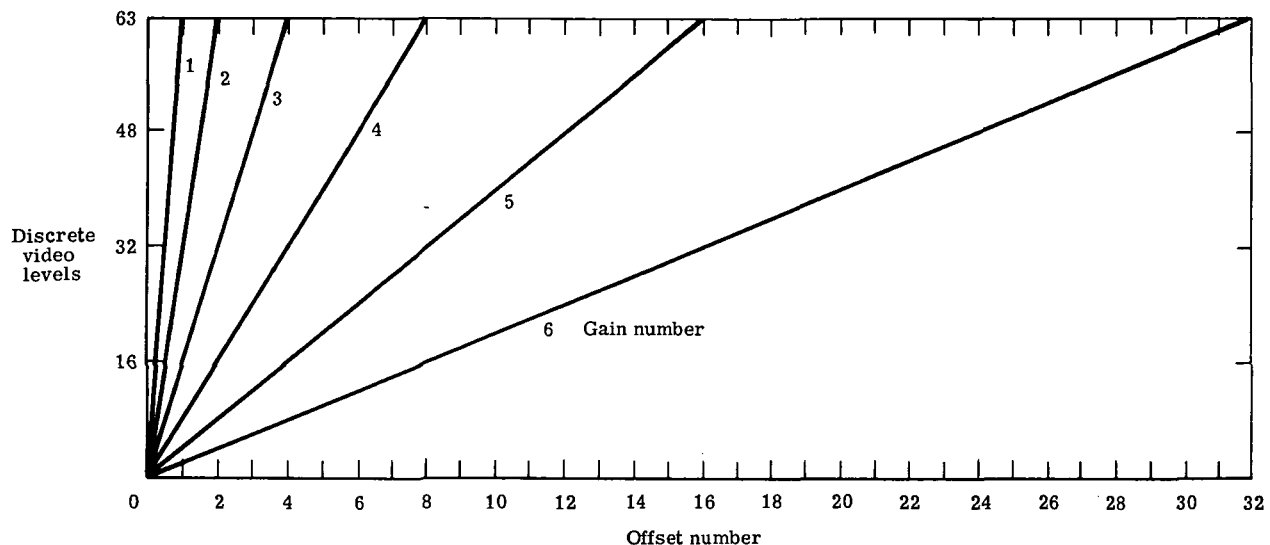
Figure 6.- Camera gains and offsets.
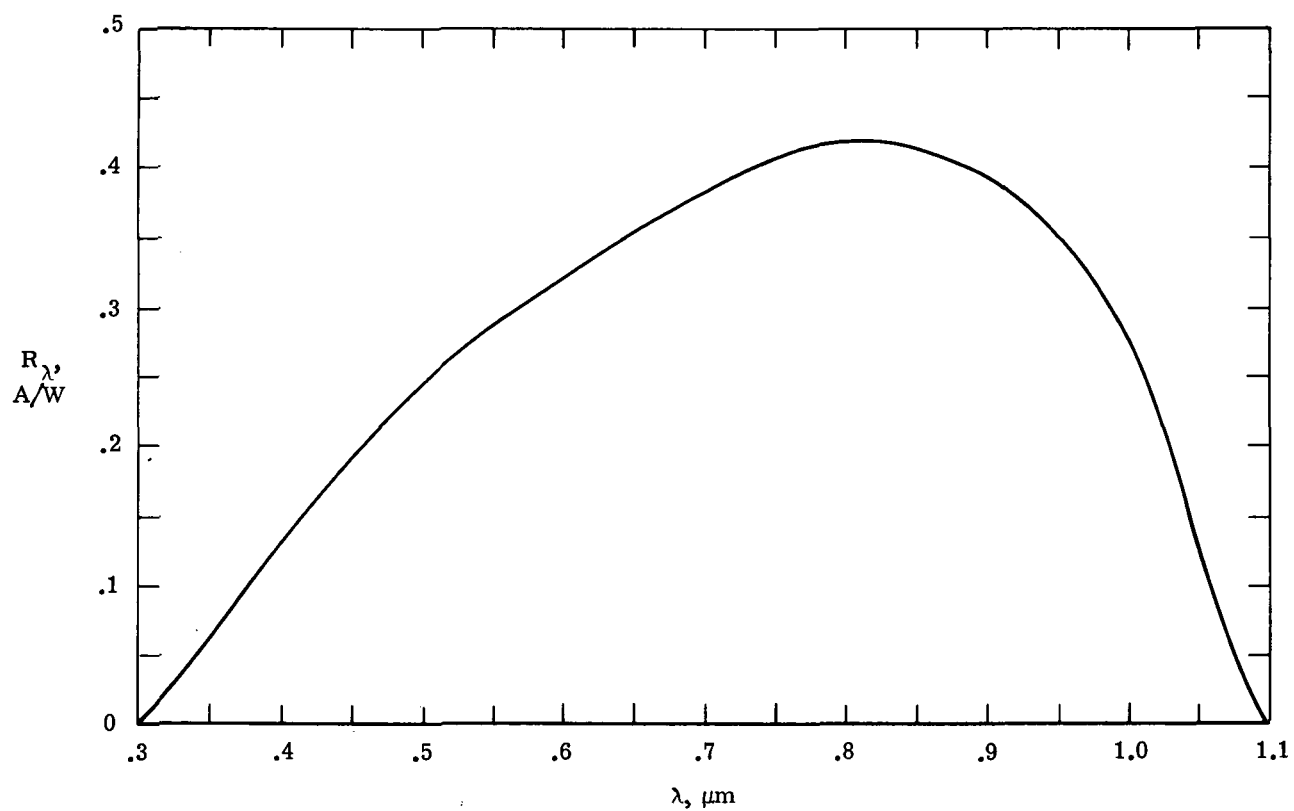
Figure 7.- Responsivity of silicon photosensor.

26
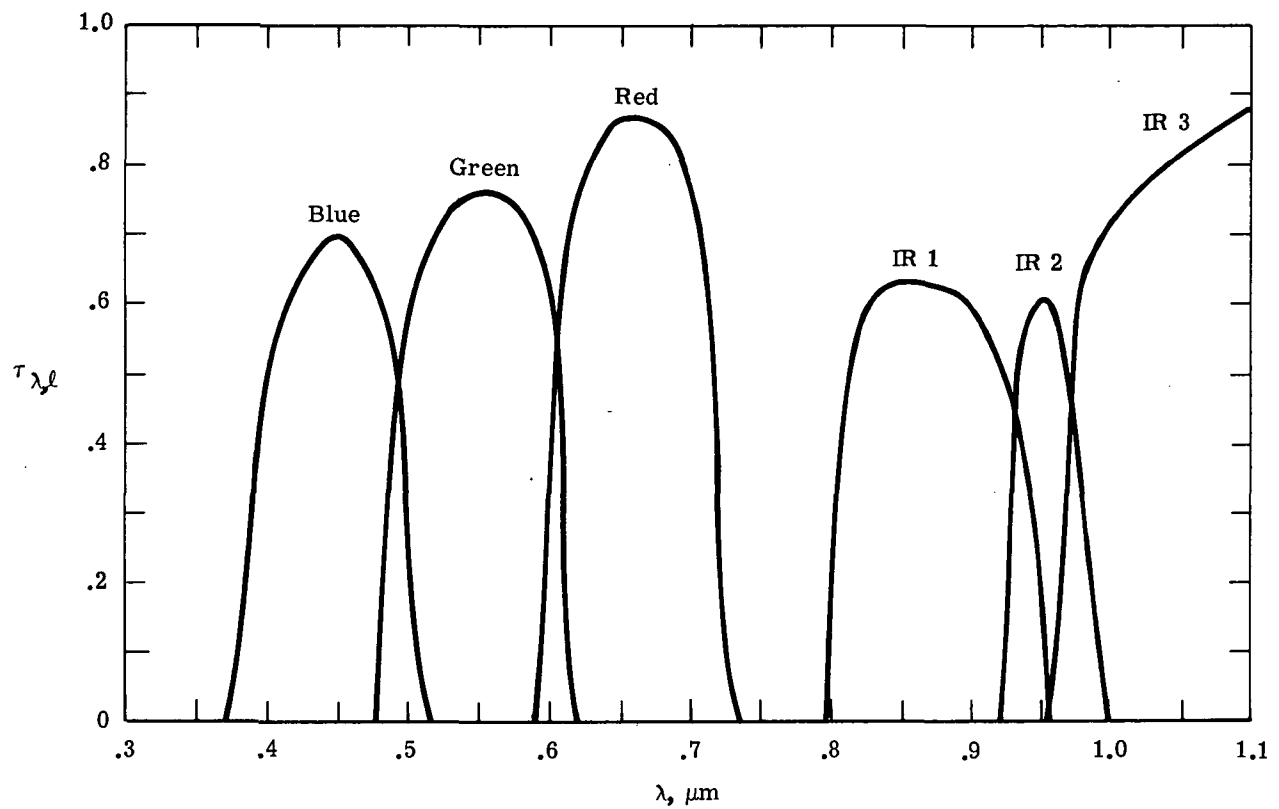
Figure 8.- Averaged transmittance of spectral filters.

"The aeronautical and space activities of the United States shall be conducted so as to contribute . . . to the expansion of human knowledge of phenomena in the atmosphere and space. The Administration shall provide for the widest practicable and appropriate dissemination of information concerning its activities and the results thereof."

—NATIONAL AERONAUTICS AND SPACE ACT OF 1958

NASA SCIENTIFIC AND TECHNICAL PUBLICATIONS

TECHNICAL REPORTS: Scientific and technical information considered important, complete, and a lasting contribution to existing knowledge.

TECHNICAL NOTES: Information less broad in scope but nevertheless of importance as a contribution to existing knowledge.

TECHNICAL MEMORANDUMS: Information receiving limited distribution because of preliminary data, security classification, or other reasons. Also includes conference proceedings with either limited or unlimited distribution.

CONTRACTOR REPORTS: Scientific and technical information generated under a NASA contract or grant and considered an important contribution to existing knowledge.

TECHNICAL TRANSLATIONS: Information published in a foreign language considered to merit NASA distribution in English.

SPECIAL PUBLICATIONS: Information derived from or of value to NASA activities. Publications include final reports of major projects, monographs, data compilations, handbooks, sourcebooks, and special bibliographies.

TECHNOLOGY UTILIZATION PUBLICATIONS: Information on technology used by NASA that may be of particular interest in commercial and other non-aerospace applications. Publications include Tech Briefs, Technology Utilization Reports and Technology Surveys.

Details on the availability of these publications may be obtained from:

SCIENTIFIC AND TECHNICAL INFORMATION OFFICE

NATIONAL AERONAUTICS AND SPACE ADMINISTRATION
Washington, D.C. 20546